Hybrid Analog-Digital Processing System for Amplitude-Monopulse RSSI-based MiMo WiFi Direction-of-Arrival Estimation

José Luis Gómez-Tornero, *Senior Member*, *IEEE*, David Cañete-Rebenaque, *Member, IEEE*, Jose Antonio López-Pastor *Student Member*, and Alejandro Santos Martínez-Sala.

***Abstract*—We present a cost-effective hybrid analog digital system to estimate the Direction of Arrival (DoA) of WiFi signals. The processing in the analog domain is based on simple well-known RADAR amplitude monopulse antenna techniques. Then, using the RSSI (Received Signal Strength Indicator) delivered by commercial MiMo WiFi cards, the DoA is estimated using the so-called digital monopulse function. Due to the hybrid analog digital architecture, the digital processing is extremely simple, so that DoA estimation is performed without using IQ data from specific hardware. The simplicity and robustness of the proposed hybrid analog digital MiMo architecture is demonstrated for the ISM 2.45GHz WiFi band. Also, the limitations with respect to multipath effects are studied in detail. As a proof of concept, an array of two MiMo WiFi DoA monopulse readers are distributed to localize the two-dimensional position of WiFi devices. This cost-effective hybrid solution can be applied to all WiFi standards and other IoT narrowband radio protocols, such us Bluetooth Low Energy or Zigbee.**

***Index Terms*—Direction of Arrival, Monopulse Antenna, RSSI-based localization, hybrid analog digital signal processing, MiMo.**

I. Introduction

Localization of mobile devices is a key enabling technology for emerging location-based applications [1], [2], cognitive radio systems [3], the Internet of Things (IoT) [4], or for future 5G systems [5]. Wireless positioning systems are based on measuring properties of the received RF signal. Basically there are three classes of RF signal quantities which are useful for a location algorithm: Direction of Arrival (DoA), Time of Arrival (ToA), and Received Signal Strength Indicator (RSSI) [6], [7]. Nowadays most of the proposed location systems with commercial hardware are based on the RSSI measurements using fingerprint techniques [8]-[11]. Acquisition and digital signal processing (DSP) of RSSI data is a cost-effective solution in commodity narrowband communication standards such as WiFi, Bluetooth Low Energy (BLE), or Zigbee. On the contrary, ToA requires accurate timing synchronization which is not possible with commodity and low-cost hardware.

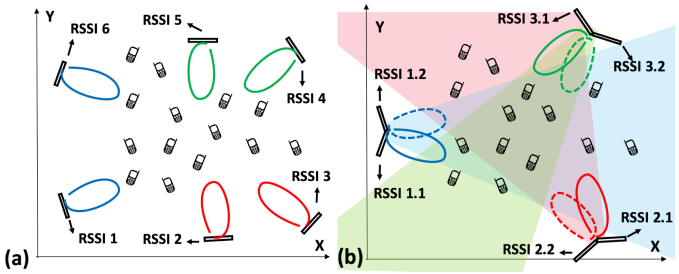

Fig. 1. Two topologies of distributed network of directive antennas for RSSI localization a) Fingerprinting technique b) HAD monopulse readers.

On the other hand, DoA estimation approaches are based on arrays of antennas distributed in the localization area as sketched in Fig.1a [12], [13]. More complex antennas technologies, such as switched beam antennas or ESPAR (Electronically Steerable Passive Array Radiators), are often combined with complex signal processing algorithms like the well-known MUSIC [14], [15] or ESPRIT [16]. These processing techniques require specific hardware to get the amplitude and phase IQ data from the RF signals, and this is not available on commodity hardware, thus becoming expensive ad-hoc solutions.

In this paper we explore a low-cost and efficient system for DoA estimation of WiFi mobile terminals based on RSSI, using a simple hybrid analog-digital (HAD) architecture. The analog signal processing (ASP) at RF frequencies is performed by pairs of tilted directive antennas following well-known amplitude-monopulse RADAR techniques [17], [18], which are recently being proposed also for localization low-cost architectures [19]-[21]. Also recent is the concept of MiMo monopulse radar [22]-[24], in which a large amount of distributed monopulse antennas can be deployed as illustrated in Fig.1b. To avoid expensive dedicated hardware which performs the monopulse comparison in the RF analog signal processing (ASP) [17]-[20], and also expensive high-performance DSP circuitry to process IQ data [25], we propose non-coherent MiMo signal processing [26] in the digital domain using the RSSI baseband data obtained from commodity MiMo WiFi hardware.

Manuscript received September 14th, 2017. This work has been supported by Spanish National projects TEC2016-75934-C4-4-R, TEC2016-76465-C2-1-R, and by Regional Seneca project 19494/PI/14.

The authors are with the Department of Information and Communication Technologies, Technical University of Cartagena (UPCT), Cartagena 30202, Spain (e-mail: josel.gomez@upct.es).

The proposed MiMo WiFi hybrid analog digital (HAD) RSSI-based monopulse DoA architecture is novel, and its presents two important features: a) its simple and low digital signal processing (DSP) computational cost since only RSSI data is needed (no IQ data), b) its robustness with respect to RSSI variations under certain conditions. As it is well-known, the use of RSSI in fingerprint-based localization schemes [8]-[11] suffer from RSSI variations due to the complex channel conditions (multipath and fading, mobility, temperature and humidity variations, inhomogeneous hardware, the relative orientation and height of the device [27]-[30]). As it will be shown, the proposed amplitude-monopulse DoA estimation technique absorbs some of the variations of RSSI, while reducing the complexity if compared to coherent DoA estimation which requires IQ data from specific hardware.

The paper is divided as follows. Section II presents the parts of the proposed MiMo WiFi HAD monopulse DoA system architecture: Section II.A describes the amplitude-monopulse antenna which performs the 2.45GHz RF analog signal processing, while Section II.B describes the analog-to-digital transformation to derive the digital MiMo WiFi monopulse DoA functions. Section III summarizes the overall hybrid AD DoA estimation performance. Special emphasis is given to the robustness and computation simplicity of this architecture if compared to other WiFi RSSI localization techniques. Finally, Section IV presents experimental results demonstrating the capability to estimate the 2D position of a user carrying a WiFi smartphone, to finalize the paper with the Conclusion Section.

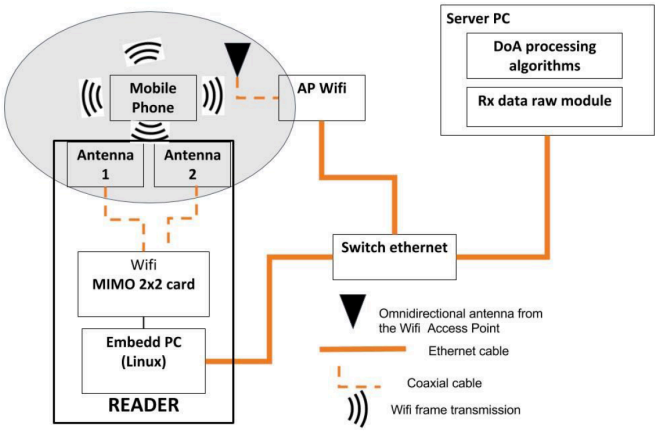

Fig. 2. Scheme of the MiMo WiFi monopulse DoA system, illustrating the ASP (Analog Signal Processing) at 2.45GHz and the DSP (Digital Signal Processing) using RSSI data collected from commercial MiMo WiFi card.

II. Hybrid Analog Digital Signal Processing for DoA

The general scheme of the proposed hybrid analog digital (HAD) architecture to estimate the Direction of Arrival (DoA) of WiFi signals is illustrated in Fig.2. The basic operations at the Reader are as follows: two commercial WiFi panel directive antennas [31] are arranged to permit monopulse analog signal processing (ASP) at RF 2.4GHz ISM band, as it will be described in detail in the next subsection II.A. A commercial 2X2 MiMo WiFi card based on Atheros AR9380 chipset [32] receives the WiFi frames signals from the monopulse antenna array and sends this raw data to an embedded Linux PC. Then the WiFi MiMo monopulse reader sends the raw data to a server by means of an Ethernet wired connection, as shown in Fig.2. Finally, the server performs the monopulse digital signal processing which will be described in subsection II.B.

A. Analog RF amplitude monopulse signal processing

The measured 2.45GHz gain pattern of the commercial panel directive antennas [31] is plotted in Fig.3a for the horizontal H-plane (XZ plane), and in Fig.3b for the vertical E-plane (YZ plane). The angle is measured with respect to the perpendicular direction of the antenna (z-axis in Fig.3). As it can be seen, this antenna provides 14 dBi gain with linearly polarized radiation (in our case vertically polarized as sketched in the inset of Fig.3). Since the maximum cross-pol level is at least 15dB below the co-pol component, only this main polarization component will be considered in the following results. The directive antenna presents a half-power beam width θ_{HPBW}=30º in both horizontal and vertical planes.

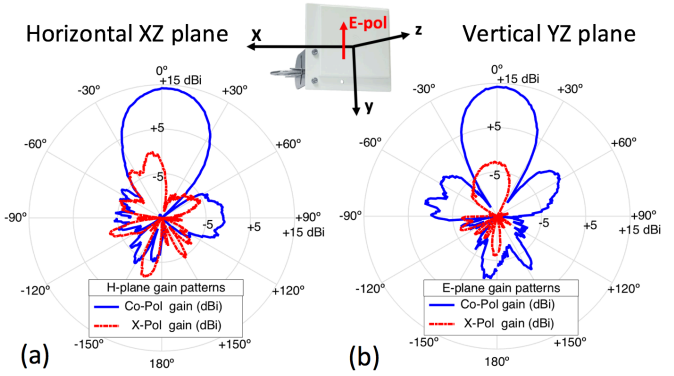

Fig. 3. Gain pattern for commercial WiFi panel antenna at 2.45GHz a) Horizontal plane b) Vertical plane. Angle θ is defined w.r.t. the z-axis.

Two panel antennas are mounted in a tripod and arranged in the x-direction side by side with a tilting angle α=7 º as shown in the inset of Fig.4. As it will be shown, this mechanical tilting must provide two mirrored radiation patterns which point to angles between one half and one third of the beam width θ_{HPBW} for an optimum monopulse response [18]. Antenna 1 is the one facing to positive azimuthal angles θ w.r.t. the z-axis (left side in Fig.4.). The gain diagrams in the horizontal XZ plane were measured for each antenna in an anechoic chamber, and they are plotted in rectangular coordinates w.r.t. the horizontal angle θ. Antenna 2 showed a lower gain (11.8 dBi) than antenna 1: this 2.4 dB gain drop is attributed to losses in the connectors. In any case, due to the geometrical tilting, the main beam of each antenna is pointing to an angle of approximately ±13 º. This angle differs from the geometrical leaning angle α=7 º due to diffraction and coupling effects in the monopulse-array system. The array half-power beam widths have also slightly varied if compared to the single antenna (to θ_{HPBW}=33 º) due to the array effects. Theoretical radiation patterns of ideal antennas with similar gains (14.2 dBi), beamwidths (33º), and scanning angles (±13 º) are also plotted with dashed lines in Fig.4.

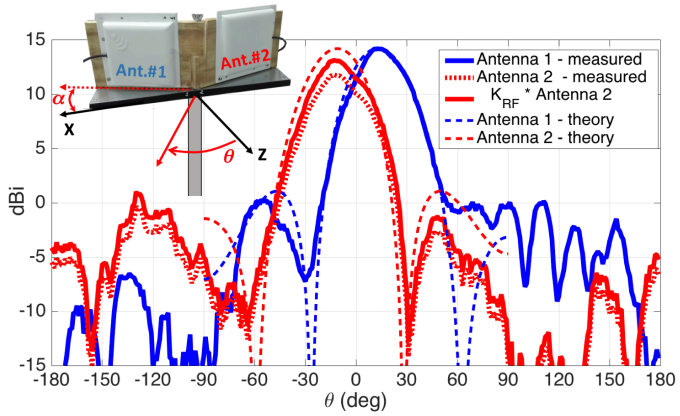

Fig. 4. Gain pattern at 2.45GHz in the horizontal plane for monopulse-array antenna system with α=7º.

This monopulse tilted-array configuration is commonly used in RADAR systems [18]. Simple analog-signal processing (ASP) is performed using the incoming RF signals amplitudes detected at each antenna. The following analog amplitude-monopulse function is defined:

$$\Psi_{RF}(\theta) = \frac{\Delta_{RF}(\theta)}{\Sigma_{RF}(\theta)} = \frac{P_{RF1}(\theta) - K_{RF} \cdot P_{RF2}(\theta)}{P_{RF1}(\theta) + K_{RF} \cdot P_{RF2}(\theta)} \quad (1)$$

where P_{RF1} and P_{RF2} are the power amplitudes –in linear form- of the RF signals received, respectively, at antenna 1 and 2 of the monopulse array. These are functions of the gain pattern of each antenna, and thus they depend on the azimuthal angle θ. Particularly, if the gain patterns of both antennas are symmetrical w.r.t. the perpendicular direction of the array θ=0º, similar RF power should be received at both antennas and the monopulse error should equal zero for a signal arriving from this perpendicular angle. However, asymmetries in the antennas gain patterns as the ones shown in Fig.4, introduce unbalance in the monopulse function. To correct for this unbalance, a compensating factor K_{RF} can be estimated from this difference in the received power at θ=0º :

$$K_{RF} = \frac{P_{RF1}(\theta=0^o)}{P_{RF2}(\theta=0^o)} \rightarrow K_{RF}(dB) = P_{RF1}(0^o) - P_{RF2}(0^o)\ (dB) \quad (2)$$

From the measured gain patterns in Fig.4, a calibration value of K_{RF}=2.4dB is obtained. Using this value in linear form (K_{RF}=1.74), the corrected power at antenna 2 ($K_{RF} \cdot P_{RF2}$) from the perpendicular direction θ=0º equals the one received by antenna 1 (as can be seen by the red continuous line in Fig.4).

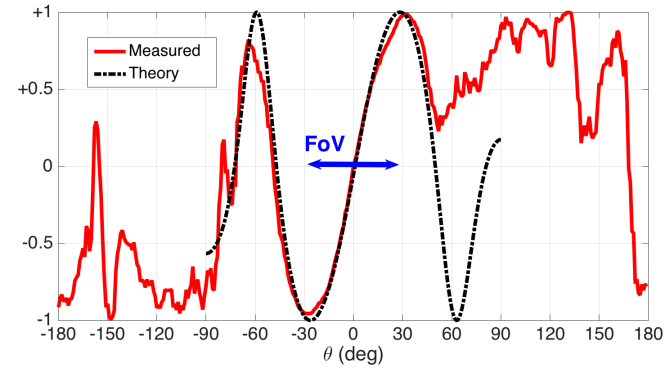

Fig. 5. Theoretical and measured analog amplitude-monopulse error functions

The corresponding analog amplitude-monopulse function (1) obtained from the measured and corrected gain patterns is shown in Fig.5. Also in this figure, the theoretical monopulse function obtained from the ideal gain patterns in Fig.4 is plotted. Good agreement is observed between theory and experiments in the analog RF domain. The Field of View (FoV) is determined by the angular region without ambiguity, so that the monopulse function presents a monotonous, quasi-linear variation from -1 to +1. It must be noticed that to obtain a proper FoV to estimate the DoA from the monopulse analog RF signal processing, the antennas radiation main beam widths and tilting angles must be properly chosen [17]. In our case, we obtain a FoV covering the angles from θ=-30º to θ=+30º. Within this range, one can estimate the DoA of an incoming signal by analog processing of the RF powers measured at each antenna of the monopulse array. First, the analog amplitude-monopulse error function $\Psi_{RF}(\theta)$ (1) has to be estimated for all possible angles θ inside the FoV. Then, for a given received RF signal, the DoA is estimated by simple comparison with $\Psi(\theta)$.

B. Digital RSSI MiMo WiFi signal processing

The objective of the proposed system is to estimate the DoA of WiFi signals transmitted from mobile devices. The angular direction is measured w.r.t. the monopulse-array plane (in our case, the horizontal plane). For this purpose, the amplitude-monopulse ASP described in the previous section, has to be extended to the reception of 2.45GHz WiFi digital frames.

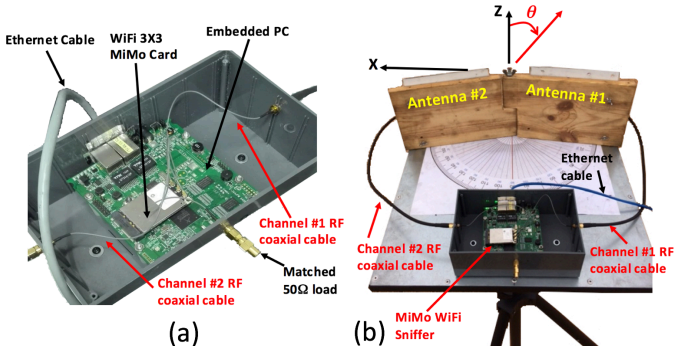

Fig. 6. a) MiMo WiFi card on embedded PC b) Monopulse MiMo WiFi reader.

As depicted in Fig.2, the mobile device (in our prototype a smartphone) is linked to a WiFi router which is transmitting WiFi frames on a regular basis. Every time the smartphone sends a WiFi frame, the reader sniffs the transmission. In more detail, the reader has a commercial MiMo 3X3 WiFi card based on AR9380 Atheros chipset [32], which is mounted on an embedded PC running Linux as illustrated in Fig.6a. This MiMO WiFi card allows connection to three different RF channels: two of them will be connected to the two antennas of the monopulse-array antenna, while the third one is matched to a 50Ω load. A sniffer program running on the embedded PC, collects the raw data from the received WiFi frames and build the raw data vector with the time stamp, reader ID, the smartphone's MAC address, and the Received Signal Strength Indicators (RSSI) measured at antenna 1 and antenna 2. This raw data is sent to the server by means of an UDP message using an Ethernet wired connection as illustrated in Fig.2.

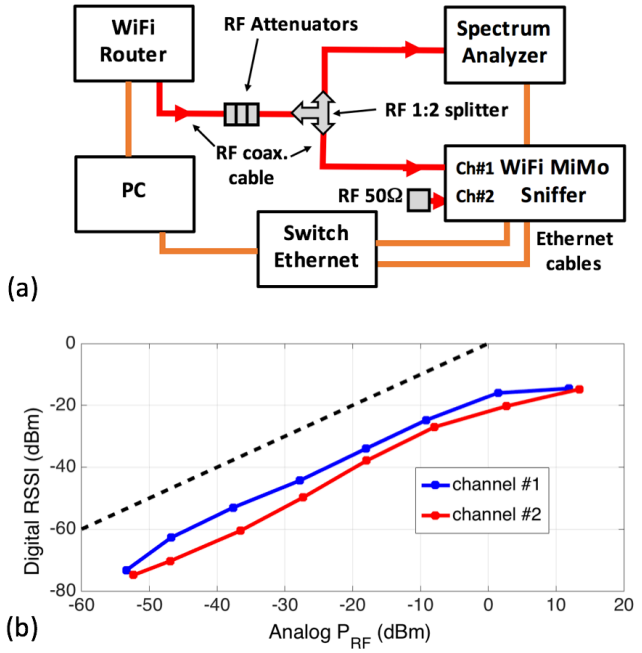

Fig. 7. Experimental characterization of the correspondence between digital power indicator RSSI and real analog RF power a) Scheme of the experimental set-up b) P_{RF}-to–RSSI plot for the two channels of the MiMo WiFi card.

The RSSI is used in many WLAN localization systems [8], [10], [11]. In our case, we want to use the RSSI as a digital estimator of the real (analog) physical RF power P_{RF} received at each antenna, assuming a linear correspondence of the form:

$$RSSI_i(\theta) = \xi \cdot P_{RFi}(\theta) \quad \text{i=1,2} \qquad (3)$$

To check the assumption in (3), a complete characterization of the correspondence between the analog RF power and the RSSI values given by the WiFi MiMO card has been performed using the test set-up sketched in Fig.7a. A WiFi router is configured to send beacon frames using IEEE 802.11g standard [33] in channel #6 frequency (2.437 GHz) with a transmitted power of 17mW and a channel bandwidth of 20MHz. The RF SMA output of the WiFi router is connected with a RF coaxial cable to a set of cascaded RF attenuators, which can provide power attenuation at a physical (analog) level ranging from 10dB to 70dB attenuation. Then, a RF 1:2 splitter T-junction is used to divide the signal in equal outputs: one is connected to a Spectrum Analyzer [34] and the other output is connected to one channel of our 2X2 MiMO WiFi reader operating in sniffer mode. The analog RF power is measured from the Spectrum Analyzer integrating the received power spectrum density with a spectral mask of 22MHz (clause 17 from [34]). Then, this power is compared with the RSSI value obtained from the WiFi MiMo reader data, obtaining the plots shown in Fig.7b for both channels of the WiFi MiMo card. All this experimental setup is controlled by a PC running Linux connected via Ethernet cable to the different test modules (see Fig.7a). By interchanging a different amount of RF attenuators, a 60dB dynamic range in the received signal power is analyzed, as shown in Fig.7b. Also in this figure, the ideal RSSI=P_{RF} function is represented in dashed line. Although there is not a 1:1 correspondence between the measured analog RF power and the digital RSSI power read by the reader, what it is important is to observe that the assumed linear dependence (3) between analog and digital figures of power is checked, and with similar slopes. However, it can be observed that the $RSSI_1$ obtained at channel#1 is 3dB above the $RSSI_2$ read at channel#2 for similar analog RF powers. Moreover, this approximate 3dB difference between the two RSSI depends on the received power, as shown in Fig.7b. Therefore, this offset is power dependent and this has to be considered in the digital signal processing of the monopulse DoA system, as it will be shown.

The RSSI angular patterns measured in an anechoic chamber are shown in Fig.8a. A smartphone transmits WiFi signals, which are received by our MiMo WiFi monopulse reader. Received WiFi frames are filtered so that only those with MAC address of the smartphone under test are processed. The $RSSI_i$ at each antenna channel (i=1,2) is measured as the relative line-of-sight (LoS) azimuthal angle θ is swept from -90º to -90º. As expected, the RSSI level received at each antenna follows the corresponding monopulse-array angular radiation patterns, which agree very well with the analog ones as compared in Fig.8b. Besides, the $RSSI_2$ signal presents a lower level than $RSSI_1$, which can be corrected applying a digital compensating factor K_D as illustrated in Fig.8a.

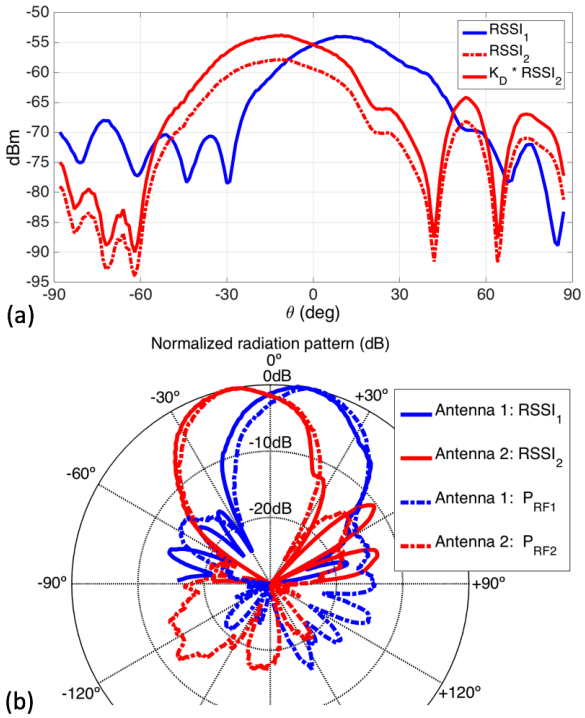

Fig. 8. a) Measured digital power (RSSI) angular patterns at the MiMo WiFi monopulse reader b) Comparison between digital (RSSI) and analog (RF power) monopulse-array normalized radiation patterns.

As done in the analog domain case, the digital correction coefficient K_D is extracted from measured $RSSI_i$ levels at the perpendicular direction θ=0º :

$$K_D = \frac{RSSI_1(\theta=0^o)}{RSSI_2(\theta=0^o)} \rightarrow K_D(dB) = RSSI_1(0^o) - RSSI_2(0^o)\ (dB) \qquad (4)$$

This digital correction must be performed for power values in a specific operating power range, since as previously

commented the power characterization shown in Fig.7b is slightly power-dependent. For that, K_D is computed by moving along the perpendicular direction in a range of distances inside the localization zone –in our case from 1 to 15 meters far from the reader-. Then, we obtain an averaged digital correction value of K_D=4dB (K_D=2.51 in linear form). This is coherent with the summation of the afore-mentioned unbalancing effects (K_{RF}=2.4dB due to asymmetries in analog-domain monopulse-array RF radiation patterns –see Fig.4, plus 2dB due to unbalance in the MiMo WiFi RSSI digital channels, see Fig.7b).

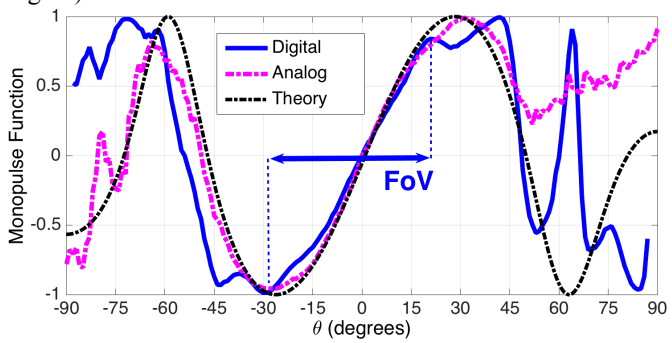

Fig. 9. Digital amplitude-monopulse function compared to its analog counterpart.

Once K_D is obtained, a digital amplitude-monopulse function can be defined from the relative RSSI values at different angles:

$$\Psi_D(\theta) = \frac{\Delta_D(\theta)}{\Sigma_D(\theta)} = \frac{RSSI_1(\theta) - K_D \cdot RSSI_2(\theta)}{RSSI_1(\theta) + K_D \cdot RSSI_2(\theta)} \quad (5)$$

This digital function is plotted in Fig.9 and it is compared with analog (1) and theoretical monopulse functions, observing good agreement. A reduced FoV of [-30º,+20º] is obtained in the digital domain. The performance of the proposed MiMo WiFi HAD monopulse architecture to estimate the DoA is studied in the next Section.

III. DoA Performance

Very simple digital signal processing is applied to estimate the DoA. Once the digital monopulse system has been calibrated by obtaining K_D (4), the amplitude-monopulse value from the received digital $RSSI_i$ data is directly computed as:

$$\Psi_{RSSI} = \frac{\Delta_{RSSI}}{\Sigma_{RSSI}} = \frac{RSSI_1 - K_D \cdot RSSI_2}{RSSI_1 + K_D \cdot RSSI_2} \quad (6)$$

Then, a simple numerical search is performed to obtain the estimated angle θ_{EST} which minimizes the following monopulse comparison error function:

$$\theta = \theta_{EST} \xrightarrow{yields} min|\Psi_D(\theta_{EST}) - \Psi_{RSSI}| \quad (7)$$

It must be noticed that this digital RSSI-based DoA estimation algorithm can be performed in real time and simultaneously for multitude of WiFi mobile terminals (each one with its corresponding filtered MAC address). This multi-user real-time capacity is possible to the reduced computational effort, since part of the signal processing is implemented in the analog domain by the RF monopulse antenna array.

The DoA estimation performance of the proposed WiFi MiMo HAD monopulse system, is studied in the following subsections with respect to different situations.

A. Quantization Error

The RSSI values obtained from the MiMo WiFi card are quantized in 1dB steps [32]. Therefore, the digital amplitude-monopulse function Ψ_D (6) is also a discretized function with a minimum step, which can be computed from the case in which the RSSI in one of the channels (for instance #1) varies in 1 dB:

$$RSSI_1'(dBm) = RSSI_1(dBm) + 1dB \rightarrow RSSI_1' = 10^{0.1} RSSI_1 \quad (8)$$

and also considering that the linear values of RSSI at each channel (after compensating channel #2 with K_D) can be related with a proportion constant χ which depends on the angle θ:

$$RSSI_1 = \chi(\theta) \cdot K_D \cdot RSSI_2 \quad (9)$$

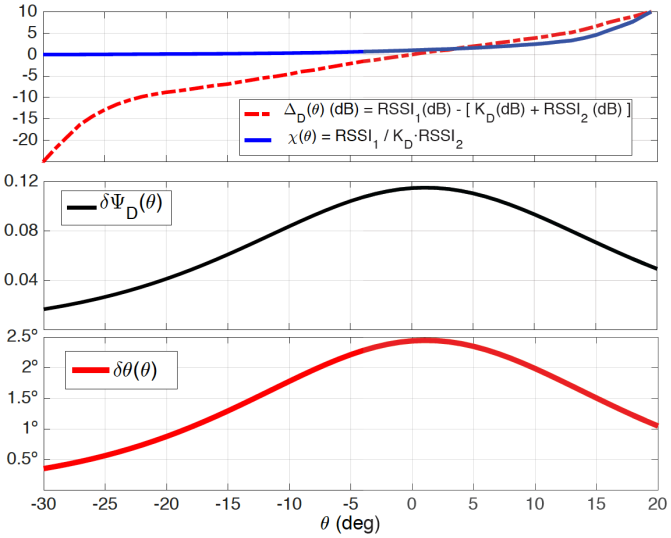

Fig. 10. Effect of the RSSI quantization in the DoA estimation error.

Obviously, $\chi(\theta)$ depends on the monopulse system digital angular pattern shown in Fig.8a, obtaining the function $\chi(\theta)$ in logarithmic and linear scales shown in Fig.10, for the angular range inside the FoV θ= [-30º,+20º]. As it can be seen, χ=1 for θ=0º, since both digital channels provide similar corrected RSSI values. At the FoV sides, χ≈10 for θ=+20º, since $RSSI_1$ is 10 dB above $RSSI_2$ due to the 10dB difference of the monopulse antenna radiation patterns (see Fig.8a), and conversely χ≈0.1 for θ=-20º since in this case $RSSI_1$ is 10 dB below $RSSI_2$. Introducing (8) and (9) in (6), the quantization error $\delta\Psi_D$, can be computed as a function of $\chi(\theta)$:

$$\delta\Psi_D(\theta) = \frac{2 \cdot \chi(\theta) \cdot (10^{0.1} - 1)}{(\chi(\theta) + 1) \cdot (\chi(\theta) + 10^{0.1})} \quad (10)$$

obtaining the result plotted in Fig.10. As shown, this quantization error is larger for perpendicular angles than for angles at the FoV sides due to the difference between the associated RSSI levels. As a result of this error $\delta\Psi_D$, the DoA angle estimated using (7) suffers an error $\delta\theta$ which again is larger for angles in the perpendicular direction than on the edges. As shown in Fig.10, $\delta\theta \approx 2.5^o$ for θ=0º, while for $\delta\theta \approx 1^o$ for θ=±20º. The digital quantization of the RSSI therefore limits

the highest theoretical resolution of this HAD monopulse DoA system to this scale. The quantized digital monopulse function showing this dependence in the angular resolution with respect to the DoA is illustrated in Fig.11.

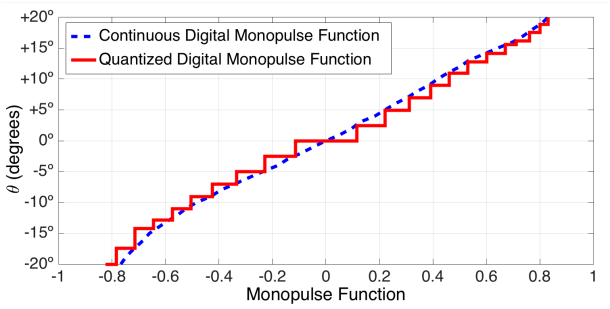

Fig. 11. Effect of the RSSI quantization in the DoA estimation error.

B. Range Variations

One of the main features of monopulse-based DoA systems is the associated robustness with respect to absolute amplitude deviations which affect both monopulse channels with the same variation level. In other words, since the monopulse function depends on the *relative* power values received between the two channels, any amplitude variation which simultaneously affects the two antennas in the same manner, will not affect the overall monopulse function. Therefore, the estimated DoA will not be affected by any signal strength variation which is sensed equally in the two channels. This is a key advantage if compared to other RSSI-based localization architectures which depend on the absolute values of RSSI [8]-[11], and which can be strongly affected by received power variations due to obstacles, orientation of the mobile device, temperature and/or humidity changes... etc [27]-[30]. Obviously, electronic noise which is uncorrelated in each reception channel cannot be absorbed by the monopulse system, and will introduce uncertainty / noise in the estimated DoA as it will be shown.

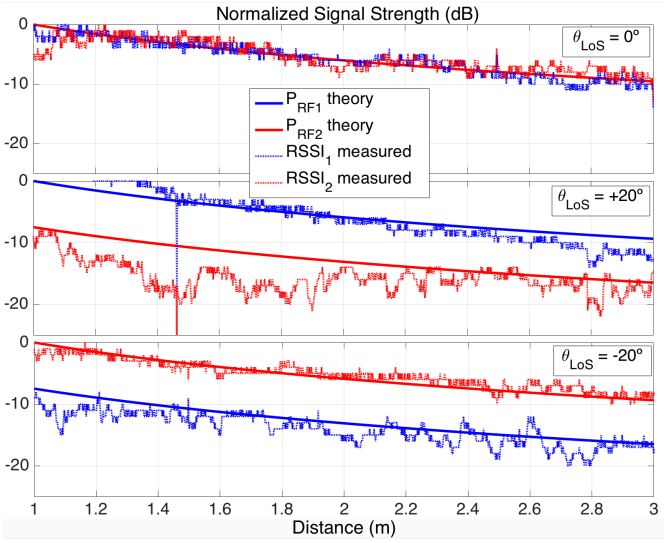

Fig. 12. Variation of the received digital power as a function of the distance and for different angular directions.

To illustrate this robustness of the estimated DoA w.r.t. absolute variations in the received power, Fig.12 shows the theoretical and measured variations for the RSSI at each channel of the MiMo WiFi monopulse reader, as a function of the distance. The experiments are performed in an anechoic chamber to minimize multipath effects, and for different line-of-sight (LOS) angular directions w.r.t. the monopulse reader, θ_{LOS}. The maximum distance was limited to 3 meters due to the anechoic chamber size. For the perpendicular direction θ_{LOS}=0º, similar values of $RSSI_i$ are received at both channels for any distance, even if the absolute values decrease with distance as predicted by theory. As a result of this similar relative values of RSSI, the theoretical amplitude monopulse value (6) should be Ψ_{RSSI}=0, leading to an estimated DoA (7) θ_{EST}=0º. However, due to system noise the monopulse function varies as can be seen in Fig.13, producing an error in the estimated DoA of ±5º. This error increases close to the reader, where the far-field tilted antenna radiation patterns used to estimate the digital monopulse function are not valid anymore.

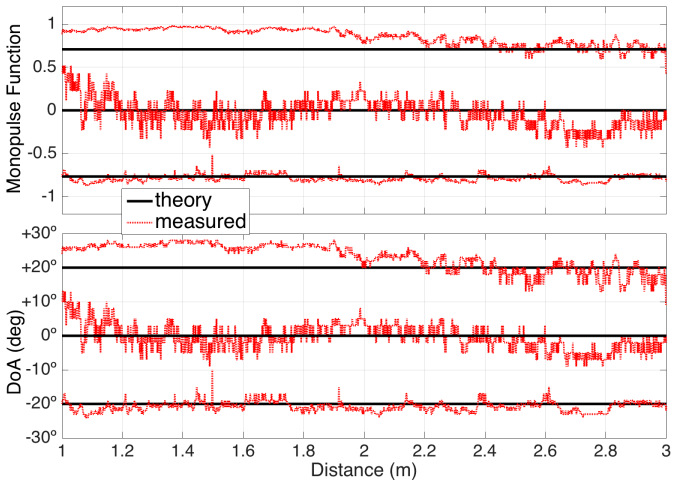

Fig. 13. Variation of the digital monopulse function and the estimated DoA as a function of the distance and for different angular directions.

For other angular directions, the expected difference in the relative RSSI levels due to monopulse angular patterns is obtained. For instance for θ_{LOS}=+20º, $RSSI_1$ is 10dB higher than $RSSI_2$ as shown in Fig.12. Moreover, this relative difference keeps almost constant for any distance, and thus the associated monopulse function value is stable around Ψ_{RSSI}=0.8 making the estimated DoA robust w.r.t. range distance variations as shown in Fig.13. Again, fluctuations are observed due to noise overlapped to quantized RSSI values, observing that this quantization error is higher for θ_{LOS}=0º than for θ_{LOS}=+20º as explained in the previous section. Similar results are obtained for θ_{LOS}=-20º, where $RSSI_1$ is 10dB lower than $RSSI_2$ for any range distance as shown in Fig.12.

C. Effect of Multipath Due to Floor

In a real scenario, multipath due to surrounding obstacles must be considered. To model the effect of reflection with floor, the setup illustrated in Fig.14 has been experimentally and theoretically analyzed. A metallic sheet has been placed on the floor of the anechoic chamber, and the distance of the WiFi mobile terminal to the reader has been varied.

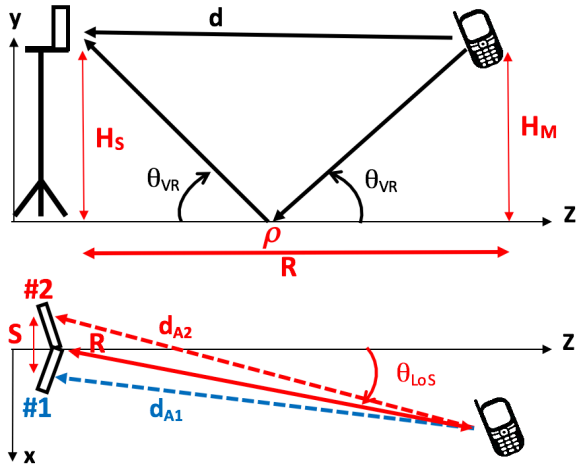

Fig. 14. Scheme of monopulse antenna array system with floor reflections.

A simple direct plus reflected ray-tracing approximation has been used to model the power received by each antenna of the monopulse array. For a given LoS direction θ_{LOS} and for any distance R between the smartphone and the center of the MiMo WiFi reader, the theoretical power received at each antenna can be computed as:

$$E_{RFi}(R) = g_i(\theta_H, \theta_V) e^{-jkd_{Ai}} \left[\frac{1}{d_{Ai}} + \frac{\rho \cdot \Delta g_{Ri}}{d_{Ai}+\Delta d_{Ri}} e^{+j(\varphi_{gRi} - k\Delta_{dRi})} \right] \quad (11)$$

$$P_{RFi}(R) = |E_{RFi}(R)|^2 \quad (12)$$

where is ρ the reflection coefficient of the floor (in our case a metallic floor ρ=-1 which is the worst case scenario), k is the free-space wavenumber at 2.45GHz, and $g_i(\theta_H, \theta_V)$ is the gain pattern of antenna i=1,2, as a function of the horizontal plane angle θ_H and the vertical plane angle θ_V. Eq.(11) includes the phase and amplitude differences of the two waves interfering at each antenna, namely the direct and the reflected waves. More particularly, the direct wave travels a distance d_{Ai} to each antenna, while the reflected wave propagates through an extra path given by Δd_{Ri}, which is computed by simple trigonometry for each antenna and for any position R and any LoS direction θ_{LOS}, taking into account the height of the reader H_S and the height of the mobile H_M (see Fig.14). Also in (11), it is considered that both waves are received at each antenna with different complex gains (amplitude and phase) due to the unequal elevation angles from which they enter the antenna, As shown in Fig.14, the direct wave enters perpendicular to the antenna elevation plane, while the reflected wave enters by an elevation angle which depends on the reflection angle θ_{VR}. This effect is modeled in (11) with an amplitude and phase difference given, respectively, by Δg_{Ri} and φ_{gRi}. Finally, it must be noticed that the distance S between the two antennas to the center of the array in the x-direction, has also been considered to compute the path lengths for each ray (see Fig.14).

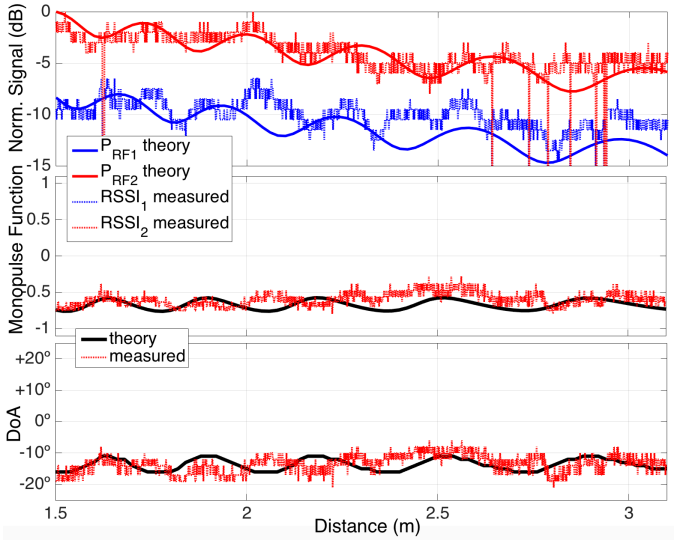

Fig. 15. Variation of RSSI, digital monopulse function and estimated DoA as a function of the distance in the presence of reflective floor for θ_{LOS}=-15º.

In our setup, S=26cm and H_S=H_M=1.5m. From the complex field due to the interference between the direct and reflected wave field (11), the power at each antenna is computed by (12). Results are plotted in Fig.15 as a function of the mobile-reader distance R from 1.5m to 3m, and for a constant horizontal angle θ_{LOS}=-15º. Measured digital RSSI levels are consistent with theoretical results.

As it can be seen, the received powers at each antenna follow a typical interference pattern, showing quasi-oscillatory behavior superposed to the monotonous decay with distance. The effect of multipath is evident if compared to Fig.12 where only direct wave was present. Most important is to understand that the monopulse system is very robust with respect to this multipath effect due to floor, since both reception channels suffer almost similar oscillatory variation. As a result, the data in the monopulse function keep almost constant as it can be seen in Fig.15. Eventually, the estimated DoA angle keeps quite stable with distance variations, showing a mean value around the real LoS angle of -15º.

D. Effect of Multipath due to Lateral Walls

Finally, the effect of multipath from lateral reflections is studied, following the scenario shown in Fig.16.

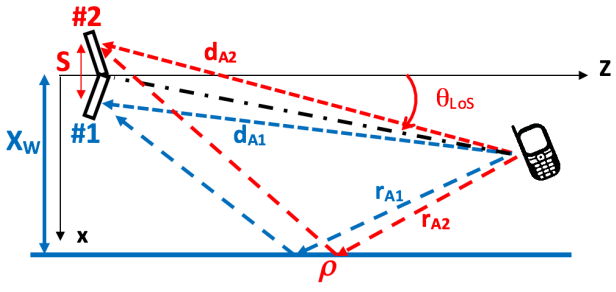

Fig. 16. Scheme of monopulse antenna array system with lateral reflections.

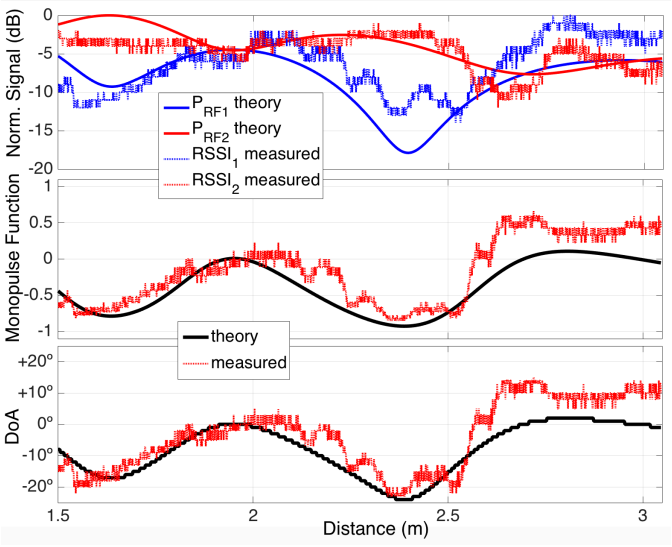

Fig. 17. Variation of RSSI, digital monopulse function and estimated DoA as a function of the distance in the presence of reflective floor for θ_{LOS}=-15º.

The key difference with respect to floor multipath, is that the interference patterns created at each monopulse channel are very distinct. Certainly, now the reflected wave produces unequal contribution for each antenna of the monopulse array. As an example, in the scheme of Fig.16, the reflected wave enters antenna #1 much more strongly than antenna #2 due to the tilted angular pattern of the monopulse array in the horizontal XZ plane. On the contrary, in the case of reflections in the floor in Fig.14, the reflected wave enters the monopulse array in a similar angle for both monopulse antennas since the multipath is produced in the vertical YZ plane and not in the horizontal ZX plane.

To illustrate this difference, Fig.17 shows the results for a similar LoS angle θ_{LOS}=-15º and similar distance variation than in the previous subsection. A metallic lateral wall is located at a horizontal distance X_W=0.8m from the reader (see Fig.16). As can be seen, now the power received at each channel behaves in a very dissimilar manner. Oscillations due to constructive and destructive interferences appear as with floor multipath: however, these oscillations are no more coherent in both channels. As a result, the relative power levels strongly vary with distance, making the monopulse function and the associated estimation of the DoA to be very sensible to distance variations. As it can be seen, the DoA given by the monopulse system shows deviations from θ_{LOS}=-20º to θ_{LOS}=+10º. Again, good agreement is observed between measured digital RSSI at each channel and simple interference theory.

Therefore, it can be concluded that the proposed MiMo WiFi HAD monopulse DoA estimation system is robust with respect to range variations if the effect of lateral obstacles is negligible. In a real indoor scenario, the monopulse technique can be combined with Neural Network post-processing in order to mitigate indoor multipath as proposed in [39].

IV. X.Y Localization

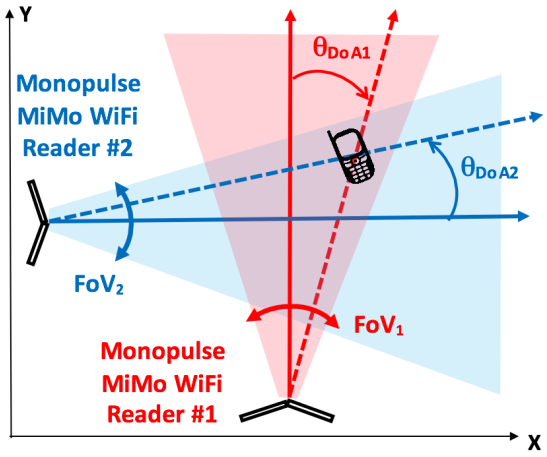

Fig. 18. Scheme of two MiMo WiFi readers to estimate X,Y coordinates.

Several readers can be located at different locations to estimate their relative DoA, and from the distributed relative data deduce the absolute position in a two-dimensional X,Y grid. As sketched in Fig.18, a minimum of two readers are needed to obtain the 2D intersection between their corresponding lines, although normally more than two DoA estimators are used for a more robust 2D localization schemes [6],[7],[19]-[24]. This way, as the number directive antennas is increased, a distributed disperse array of antennas must be somehow deployed in the area, as it was shown in Fig.1. The collected RSSIs from all the readers are then processed by the server to estimate the positions of the mobile terminals using different algorithms, most of them, fully digital, based on RSSI fingerprints [8]-[11].

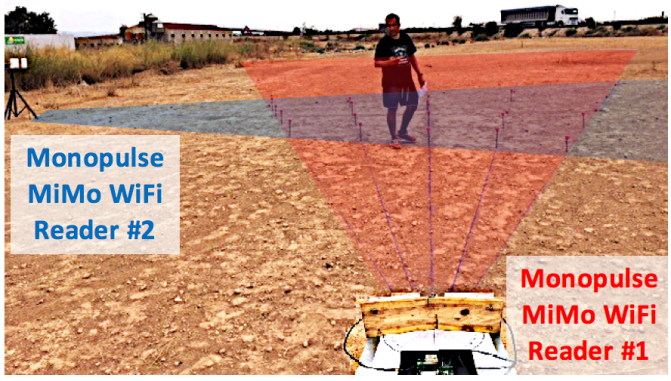

Fig. 19. Picture of two MiMo WiFi monopulse readers deployed in outdoors.

In our case, the monopulse antenna array from each reader defines a triangle by its respective orientation and Field of View (FoV). As illustrated in Fig.18 for the case of two readers, the shadowed intersection zone is the region where WiFi devices can be localized without ambiguity by using the proposed simple HAD monopulse technique. Fig.19 shows a picture of a real outdoor deployment of two monopulse readers in a rural area. The two readers are orthogonally (90º) located following the scheme in Fig.18, so that the center of the localization region defines the origin of the absolute X,Y coordinate system, which is at a distance of 8 meters from each reader.

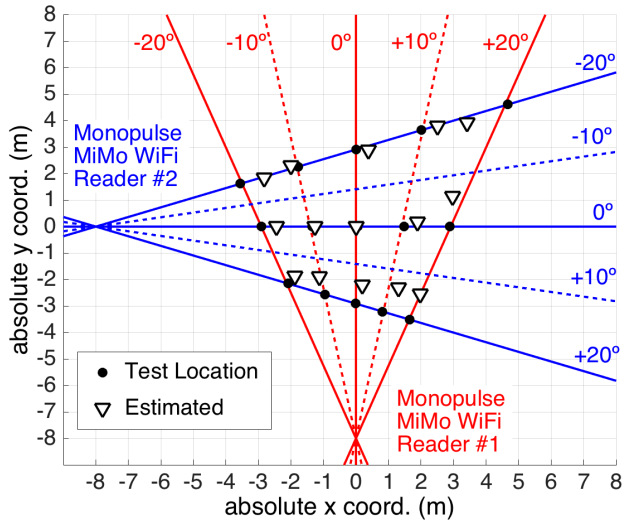

Fig. 20. X,Y localization performance.

In the outdoor experiment, 15 test points were located at the intersections between the relative equiangular lines of -20º,-10º,0º,+10º,+20º of the two monopulse readers. It must be observed that these test points are not symmetrically located w.r.t. the readers in Cartesian coordinates. For all these test points, the DoA estimated by each MiMo WiFi reader was computed in real time and processed by a local server, which ultimately predicted the estimated X,Y position. The results for the 15 test points at the intersections of the central lines (θ=0º) and edge lines (θ=±20º) of the two readers FoVs are summarized in Fig.20. The test points are represented with circles, and the estimated positions with triangles. The mobiles positions are tracked in real time, with extreme simplicity and average accuracy of 1 meter, which is consistent with the reported 5deg DoA average accuracy and the distances in this experiment. Obviously, for a similar angular resolution, the X,Y localization error is higher as the distance to the DoA monopulse reader increases. As a result, the localization error is greater for the furthest test location (intersection between reader #1 +20º line and reader #2 -20º line, see Fig.20), where an error of 1.5 meters is obtained.

Finally, the robustness of this DoA estimation system with respect to the relative position of the WiFi device, is studied. For that purpose, the received RSSI signals are analyzed in a period of 40 seconds in which the device holder sequentially moves the smartphone among three different common uses: speaking, reading and smartphone hidden inside a trousers pocket. These three uses are coded as A, B and C, respectively, in the inset of Fig.21. As shown, the RSSI shows a 15dB drop when the mobile is inside the pocket, while slighter variations are observed between speaking and reading modes. Nevertheless, what is again important is to observe that the RSSI levels measured by the two channels of each monopulse array vary in the same manner, leading to almost null *relative (differential)* RSSI variation. As explained previously, this keeps the monopulse function almost unchanged despite this type of signal variations, and so does the estimated DoA, as it can be seen in the measured results in Fig.21.

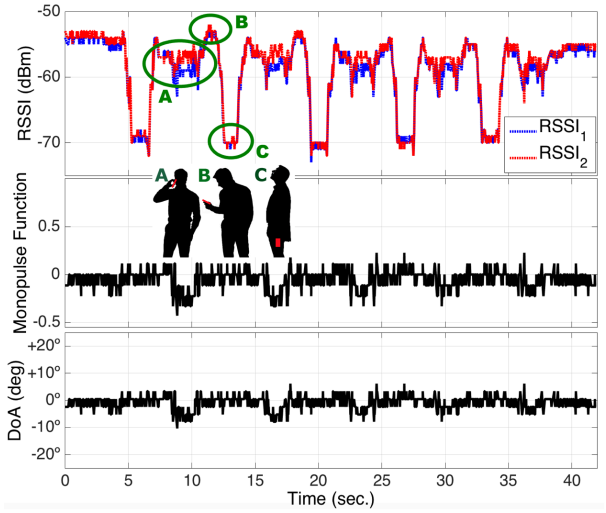

Fig. 21. Variation of RSSI, monopulse function and estimated DoA as the smartphone is modified from speaking, reading and hidden-in-pocket modes.

Similar results are obtained when the relative orientation of the mobile terminal is modified, i.e., when the person changes facing forward, backward and lateral w.r.t the monopulse readers. Again, this robustness w.r.t mobile orientation changes is explained from the fact that these variations alter to the same extent the RSSI at both channels of each monopulse reader, thus keeping stable the estimated DoA. Similar stability with respect to humidity, temperature and other RF channel fluctuations is expected, thus being superior in this aspect than RSSI-fingerprint-based techniques [27]-[30].

Certainly, this robustness is achieved thanks to the use of analog RF monopulse techniques which gather each pair of antennas of the total distributed antenna network in a more efficient manner. As illustrated in Fig.1b and described in Section II.A, each pair of directive antennas must be arranged together and geometrically tilted to a given angle α (which depends on their directive beam half power beam-width θ_{HPBW}), so that their radiation patterns properly overlap and produce an adequate monopulse function with their respective FoV. As an example, Fig.22 illustrates the dependence of the analog RF monopulse function for directive antennas with θ_{HPBW}=35º (similar to the ones used in this work), and for different geometrical leaning angles α (which turn into different angles of maximum radiation of their respective radiation patterns θ_M).

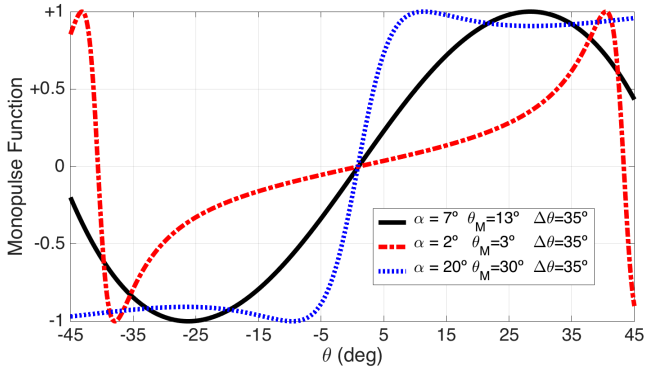

Fig. 22. Dependence of the analog RF monopulse function for two directive antennas with θ_{HPBW}=35º, and for different geometrical tilting angles.

Table I – Comparison between the proposed WiFi HAD monopulse DoA architecture and other WiFi localization metric alternatives.

REF	Architecture	Performance	Complexity
[8], [35]-[41]	Only RSSI-based fingerprinting system	Meters indoor	Medium. RSSI acquisition is simple. Exhaustive data acquisition training phase, and need of classification algorithms
[42],[43]	CSI-based phased-antenna techniques for DoA estimation	Centimeters indoor	High. Phase information (CSI) required. Hardware and software modifications for accurate phase-delay measurement.
[44]	CSI-based MUSIC algorithm for DoA and ToA estimation	Decimeters indoor	High. Phase information (CSI) required. MUSIC algorithm to estimate ToA and DoA.
[45],[46]	CFR-based fingerprinting system	Centimeters indoor	High. Channel Frequency Response (CFR) required. Exhaustive data acquisition training phase, and need of classification algorithms.
this paper	RSSI-based DoA estimation using monopulse technique	Decimeters outdoor	Low. RSSI acquisition is simple. No need of exhaustive data acquisition and training phase, only calibration of correction factor. No need of classification algorithms to estimate the DoA.

As it can be seen, the slope of the analog monopulse function can be engineered, so that higher values of α produce stepper angular monopulse responses (see blue dotted line in Fig.22). This reduces the FoV, but increase the angular resolution since the angular error due to digital quantization is reduced, as explained in Section III.A. Conversely, less tilted antennas (lower α) increase the FoV at the cost of higher angular error / less angular resolution, as shown in red dashed line in Fig.22.

V. Comparison with State-of-the-Art Alternatives

A concluding Table I compares the proposed HAD DoA architecture with other alternatives found in the literature, in terms of localization performance and simplicity. The RSSI metric has been extensively used for fingerprinting-based WiFi localization algorithms ([8], [35]-[41]). These RSSI-based fingerprinting techniques do not estimate the DoA of the signals. They only use the signal strengths to construct power-based RSSI radiomaps.

The combination of different metrics (RSSI, DoA and ToA) have demonstrated superior performance if compared to only-RSSI based fingerprinting localization systems. For this reason, the estimation of the DoA has been pursued in many WiFi localization architectures [42]-[46]. In this context, WiFi is not compatible with ultrawideband DoA techniques which require high-bandwidth (such as [47] and [48]), which is not available in WiFi technologies. To estimate the DoA in WiFi systems, previous proposals rely on phase-delay information which requires much more complex IQ hardware than solutions based only on RSSI (amplitude information). For instance, ArrayTrack [42] and Phaser [43] estimate the DoA using phased-array antenna techniques based on CSI (Channel State Information) acquisition and processing. In the same manner, Spotfi [44] estimates the DoA and the ToA using CSI data and super-resolution MUSIC algorithms. In any case, CSI data is not available in commodity hardware, and hardware/software modifications are requested to solve the differences in phase of the oscillators for accurate phase-delay prediction. Therefore, these CSI-based DoA architectures [42]-[44] are more complex solutions than those based only on RSSI as the one proposed in this paper. Finally, other WiFi localization solutions are based on processing of the CFR (Channel Frequency Response) for multiple frequency channels [45], or for multiple antennas [46]. Again, the CFR acquisition relies on specific hardware and software. Also, to construct the CFR radiomap, an exhaustive data acquisition training phase is requested, and an algorithm is necessary to compensate residual synchronization errors.

For all these reasons, the RSSI-based DoA monopulse architecture proposed in this work is much simpler, since it relies on direct measurement of the RSSI, and it does not need extra training or calibration phase for precise IQ data processing. In our case, the simple estimation of the afore described correction factor is sufficient as demonstrated in this paper. However, this simplicity provides lower resolution (in the order of +-2.5º) and lower robustness w.r.t. indoor multipath effects, than more complex DoA CSI/CFR-based techniques [42]-[46]. In future works, the monopulse technique will be combined with machine learning algorithms in order to mitigate indoor multipath as proposed in [39], [49], and envisage a complete WiFi indoor localization system based on this architecture fusion with fingerprinting techniques. Moreover, heterogeneous networks (WiFi plus cellular) information can be combined for enhanced positioning performance [50], [51].

VI. CONCLUSION

We have presented a cost-effective hybrid analog digital monopulse system where MiMo WiFi readers estimate the Direction of Arrival (DoA) of RF transmissions from smartphones. The reader has a commercial MiMo WiFi card with attached directive antennas in a tilted monopulse configuration. The processing in the analog domain is based on simple well-known RADAR amplitude monopulse antenna techniques. On the digital domain, the reader monitors the WiFi frames transmitted from each device and measures its RSSI (Received Signal Strength Indicator). Then, the DoA is estimated using the so-called digital monopulse function. Finally, as a proof-of-concept, two readers operating at 2.45GHz are distributed outdoors in order to localize the two-dimensional position of a person carrying a smartphone. In spite of using commodity hardware, we demonstrate that the DoA estimation is robust against the RSSI fluctuations produced by the smartphone orientation, floor multipath effects and range variations. Due to the hybrid analog digital architecture, the digital processing of the DoA is extremely simple with reduced computational cost and can enrich the widely proposed WiFi RSSI-based fingerprinting location systems. Currently, the proposed RSSI-based HAD monopulse architecture is being developed for tracking WiFi smartphones in open wide-area mass events, and also for IoT devices based on Bluetooth Low Energy and Zigbee.

REFERENCES

[1] R. Zekavat, and R.M. Buehrer. *Handbook of position location: Theory, practice and advances*. vol. 27. John Wiley & Sons, 2011.

[2] K. W. Kolodziej, J. Hjelm, Local Positioning Systems: LBS Applications and Services, ed. CRC, 2006

[3] H. Celebi, and H. Arslan. "Utilization of location information in cognitive wireless networks." *IEEE Wireless Communications* 14.4 (2007).

[4] D. Macagnano, G. Destino, and G. Abreu, "Indoor positioning: A key enabling technology for IoT applications." *Internet of Things (WF-IoT), 2014 IEEE World Forum on*. IEEE, 2014.

[5] M. Koivisto, et al. "High-efficiency device positioning and location-aware communications in dense 5G networks." *IEEE Communications Magazine*, 2017.

[6] A. Bensky, *Wireless positioning technologies and applications*. Artech House, 2016.

[7] H. Liu, H. Darabi, P. Banerjee, and J. Liu, "Survey of wireless indoor positioning techniques and systems", *IEEE Transactions on Systems, Man, and Cybernetics*, Part C (Applications and Reviews), vol. 37, no. 6, pp. 1067-1080, 2007.

[8] S. He, andS. H. G. Chan, "Wi-Fi fingerprint-based indoor positioning: Recent advances and comparisons", IEEE Communications Surveys & Tutorials, vol.18, no.1, pp. 466-490, 2016.

[9] R. Guzmán-Quirós, A.J. Martínez-Salas, J. L. Gómez-Tornero, and J. García-Haro, "Integration of directional antennas in an RSS fingerprinting-based indoor localization system," in *Sensors, Special Issue Sensors for Indoor Mapping and Navigation*, vol. 16, no. 4, pp. 1-23, December 2015.

[10] Q.D. Vo, and P. De, "A survey of fingerprint-based outdoor localization." *IEEE Communications Surveys & Tutorials* vol.18, no.1, pp. 491-506, 2016.

[11] A. Yassin, et al. "Recent advances in indoor localization: A survey on theoretical approaches and applications." *IEEE Communications Surveys & Tutorials*, vo.19, no.2, pp. 1327-1346, 2016.

[12] L. Brás, N. Borges-Carvalho, P. Pinho, L. Kulas, and K. Nyka, "A review of antennas for indoor positioning systems," *International Journal of Antennas and Propagation*, vol. 2012.

[13] J. Werner, J. Wang, A. Hakkarainen, N. Gulati, D. Patron, D. Pfeil, K.R. Dandekar, D. Cabric, M. Valkama "Sectorized Antenna-based DoA Estimation and Localization: Advanced Algorithms and Measurements," *IEEE Journal on Selected Areas in Communications*, vol. 33, no. 11, pp. 2272-2286 2015.

[14] R. O. Schmidt, "Multiple emitter location and signal parameter estimation," IEEE Transactions on Antennas and Propagation, vol. 34, no. 3, pp. 276–280, 1986.

[15] A. Y. J. Chan and J. Litva, "MUSIC and maximum likelihood techniques on two-dimensional DOA estimation with uniform circular array," IEE Proceedings, vol. 142, no. 3, pp. 105–114, 1995.

[16] R. Roy, A. Paulraj, and T. Kailath, "ESPRIT—a subspace rotation approach to estimation of parameters of sinusoids in noise," IEEE Transactions on Acoustics, Speech, and Signal Processing, vol. 34, no. 5, pp. 1340–1342, 1986.

[17] E. Mosca, "Angle estimation in amplitude comparison monopulse systems," *IEEE Transactions on Aerospace and Electronic Systems*, vol. AES-5, no. 2, pp. 205–212, Mar. 1969.

[18] S.M. Sherman and D.K. Barton, *Monopulse Principles and Techniques*, Artech House Radar Library. Artech House, 2011

[19] J. C.Wu, C. C. Chang, T. Y. Chin, S. H. Chang,M. C. Chiu, C. Y. Hsu, and R. H. Lee, "Wireless indoor localization using dynamic monopulse receiver," in *EURAD 2010*, pp. 69–72.

[20] M. Del Prete, D. Masotti, N. Arbizzani and A. Costanzo, "Remotely identify and detect by a compact reader with mono-pulse scanning capabilities," in *IEEE Trans. on Microwave Theory and Techn.*, vol. 61, no. 1, pp. 641-650, Jan. 2013.

[21] B. Denis, B. Uguen, F. Mani, R. D'errico, N. Amiot, "Joint orientation and position estimation from differential RSS measurements at on-body nodes", *IEEE 27th Annual International Symposium on Personal Indoor and Mobile Radio Communications* (PIMRC) pp. 1-6, 2016.

[22] S. Gogineni, A. Nehorai, "Target tracking using monopulse MIMO radar with distributed antennas", *Radar Conference 2010 IEEE*, pp. 194-199, 2010

[23] S. Gogineni and A. Nehorai, "Monopulse MIMO Radar for Target Tracking," in *IEEE Transactions on Aerospace and Electronic Systems*, vol. 47, no. 1, pp. 755-768, Jan. 2011.

[24] S. Jardak, S. Ahmed, M.-S. Alouini, "Two target localization using passive monopulse radar", *Radar Conference 2015 IEEE*, pp. 191-196, 2015.

[25] L. Pang, F-B. Mao, Y.-Z. Xie, H. Chen, "A high performance digital signal processor for monopulse tracking radar", *Signal Processing (ICSP) 2016 IEEE 13th International Conference on*, pp. 1485-1488, 2016

[26] Q. He, R.S. Blum, "Noncoherent versus coherent MIMO radar: Performance and simplicity analysis", *Signal Processing*, vol. 92, pp. 2454, 2012.

[27] C. Wu, et al. "Mitigating large errors in wifi-based indoor localization for smartphones." *IEEE Transactions on Vehicular Technology* 66.7 (2017): 6246-6257.

[28] Y. Chapre, et al. "Received signal strength indicator and its analysis in a typical WLAN system (short paper)." *Local Computer Networks (LCN), 2013 IEEE 38th Conference on*. IEEE, 2013.

[29] K. Kaemarungsi, and P. Krishnamurthy, "Analysis of WLAN's received signal strength indication for indoor location fingerprinting". *Pervasive and Mobile Computing*. 2012, 8, 292–316.

[30] J. Luo, J.; Zhan, X. "Characterization of Smart Phone Received Signal Strength Indication for WLAN Indoor Positioning Accuracy Improvement". *Journal of Networks*. 2014, *9*, 739–746.

[31] Interline 14dB panel antenna IP-G14-F2425-H, datasheet available online at: http://www.interline.pl/antennas/PANEL-14-2.4GHz

[32] Atheros AR9380 chipset datasheet, available online at: https://wikidevi.com/files/Atheros/specsheets/AR9380.pdf

[33] IEEE 802.11.g-2003 standard, available online at: http://standards.ieee.org/getieee802/download/802.11g-2003.pdf

[34] Rodhe&Schwarz ZVL6 Vector Network Analyzer, available online at: http://www.testequipmenthq.com/datasheets/Rohde-Schwarz-ZVL6-Datasheet.pdf

[35] P. Bahl, and V.N. Padmanabhan, "RADAR: an in-building RF-based user location and tracking system", *In Proceedings IEEE INFOCOM, vol. 2,* pp. 775–784, 2000.

[36] P. Bahl, V.N. Padmanabhan, and A. Balachandran. "Enhancements to the RADAR user location and tracking system." *Microsoft Research 2*. MSR-TR-2000-12. pp.775-784, 2000

[37] P. Müller, M. Raitoharju, and R. Piché, "A field test of parametric WLAN-fingerprint-positioning methods," in *Proc. 17th Int Conf. Inf. Fusion*, pp. 1–8, 2014.

[38] A. Khalajmehrabadi, N. Gatsis, And D. Akopian, "Modern WLAN Fingerprinting Indoor Positioning Methods and Deployment Challenges", *IEEE Communications Surveys & Tutorials*, 19(3), pp. 1974–2002. 2017

[39] P. Davidson, and R.A. Piche, R. "A Survey of Selected Indoor Positioning Methods for Smartphones", *IEEE Communications Surveys & Tutorials*, 19(2), 1347–1370, 2017.

[40] Q.D. Vo, and P. De, "A Survey of Fingerprint-Based Outdoor Localization", *IEEE Communications Surveys & Tutorials*, 18(1), 491–506, 2016.

[41] Y. Feng et al., "An improved indoor localization of WiFi based on support vector machines," *Int. J. Future Gener. Commun. Netw.*,vol.7, no. 5, pp. 191–206, 2014.

[42] J. Xiong, and K. Jamieson, ArrayTrack: A Fine-Grained Indoor Location System", *USENIX Symposium on Networked Systems Design and Implementation*, pp .71–84, 2013

[43] J. Gjengset, J. Xiong, G. McPhillips, and K. Jamieson, "Phaser: Enabling Phased Array Signal Processing on Commodity WiFi Access Points", *in Proceedings of the 20th annual international conference on Mobile computing and networking - MobiCom '14*, pp. 153–164, 2014.

[44] M- Kotaru, K. Joshi, D. Bharadia, and S. Katti, "Spotfi: Decimeter level localization using WiFi". *In ACM SIGCOMM Computer Communication Review* (Vol. 45, No. 4, pp. 269-282). ACM. 2015.

[45] C. Chen, Y. Chen, Y. Han, H.-Q. Lai, H.-Q., and K.J.R. Liu, "Achieving Centimeter Accuracy Indoor Localization on WiFi Platforms: A Frequency Hopping Approach", *IEEE Internet of Things Journal,* vol 4, pp. 111-121., 2017

[46] C. Chen, Y. Chen, Y. Han, H.-Q. Lai, H.-Q., and K.J.R. Liu, "Achieving Centimeter Accuracy Indoor Localization on WiFi Platforms: An Multi-Antenna Approach", *IEEE Internet of Things Journal*, vol 4, pp 122-134. 2016.

[47] A. Hirata, T. Morimoto, and Z. Kawasaki, "DOA estimation of ultra-wideband EM waves with MUSIC and interferometry ", *IEEE Antennas and Wireless Propagation Letters*, pp 190–193. 2003

[48] M. Wang, S., Yang, S. Wu, and F. Luo, F.. "A RBFNN approach for DoA estimation of ultra wideband antenna array", *Neurocomputing,* pp. 631–640. 2008

[49] S. Mishra, R.N., Yadav, and R.P. Singh, "A Survey on Applications of Multi Layer Perceptron Neural Networks in DOA Estimation for Smart Antennas", *International Journal of Computer Application,* pp. 22–28. 2013.

[50] M. Laaraiedh, S. Avrillon and B. Uguen, "Enhancing Positioning Accuracy through Direct Position Estimators Based on Hybrid RSS Data Fusion," *VTC Spring 2009 - IEEE 69th Vehicular Technology Conference*, pp. 1-5, 2009.

[51] A. Yassine, Y. Nasser, M. Awad, and B. Uguen, "Hybrid positioning data fusion in heterogeneous networks with critical hearability", *Eurasip Journal on Wireless Communications and Networking*, pp. 1–16. 2014.

José Luis Gómez-Tornero (SM'01–M'06–SM'14) was born in Murcia, Spain, in 1977. He received the Telecommunications Engineer degree from the Technical University of Valencia, Valencia, Spain, in 2001, and the Ph.D. degree from the Technical University of Cartagena (UPCT), Cartagena, Spain, in 2005. In 2000, he joined the Radio Frequency Division, Industry Alcatel Espacio, Madrid, Spain. In 2001, he joined UPCT, where he has been an Associate Professor since 2008. He was Vice Dean for Students and Lectures affairs as a member of the Telecommunication Engineering Faculty. He has been a Visiting Researcher/Professor with the University of Loughborough, Loughborough, U.K., Heriot-Watt University, Edinburgh, U.K., Queen's University of Belfast, Belfast, U.K., and CSIRO-ICT Centre, Sydney, N.S.W., Australia. In February 2010, he was appointed a CSIRO Distinguished Visiting Scientist by the CSIRO ICT Centre.

He has co-authored more than 50 peer-reviewed journal papers, and more than 100 conference papers. His current research interests include the analysis and design of leaky-wave devices and their applications, and the innovation in the area of higher education.

His research work has received various awards, including EPSON-Ibérica foundation (2004) and Vodafone Foundation (2005) awards to the best Ph.D. thesis in the area of advanced mobile communications technologies, Hispasat (2014) and Hisdesat (2015) prizes to the best Ph.D. thesis in Satellite Communication technologies. Also, he was the co-recipient of the 2010 IEEE Engineering Education Conference Award, the 2011 EuCAP Best Student Paper Prize, the 2012 EuCAP Best Antenna Theory Paper Prize, the 2012 and 2013 Spanish URSI Prize for the best student paper, the 2013 APS Best Student Paper finalist, and the 2018 iWAT Best Poster award.

David Cañete-Rebenaque was born in Valencia, Spain, in 1976. He received the Telecommunications Engineer degree from the Technical University of Valencia, Valencia, Spain, in 2000, and the Ph.D. degree from the Technical University of Cartagena, Cartagena, Spain, in 2009. During 2001, he was an RF Engineer with a mobile communication company. In 2002, he joined the Communications and Information Technologies Department, Technical University of Cartagena, where he is involved with research and teaching activities. His research interests include the analysis and design of planar microwave circuits and antennas.

José A. López-Pastor received the B.S. degree in telematics engineering in 2006 and M.S. degree in telecommunication engineering in 2010 from the Universidad Politecnica de Cartagena (UPCT), Cartagena, Spain. After 8 years working in private R&D technological center, he started Ph.D degree at Universidad Politécnica de Cartagena (UPCT). His research interest includes indoor positioning system, software programming and IoT.

Alejandro S. Martinez-Sala was born in Cehegin, Spain, in 1976. He received the Electrical Engineering degree in 2000 and the Ph.D. in Telecommunications from the Technical University of Cartagena (UPCT), Spain, in 2006. In 2001 he joined the UPCT where he is assistant professor at the Communications and Information Technologies Department. His research interests include the indoor location systems, wireless sensor networks, and innovation and technology transfer.